

Electronic supplementary information

Experimental section

Materials: Nickel nitrate hexahydrate ($\text{Ni}(\text{NO}_3)_2 \cdot 6\text{H}_2\text{O}$), sulfur (S) and cerium sulfate tetrahydrate ($\text{CeS}_2\text{O}_8 \cdot 4\text{H}_2\text{O}$) were purchased from Aladdin Ltd (Shanghai, China). Hexamethylene tetramine (HMT) was purchased from Beijing Chemical Corporation. Nafion 117 solution was purchased from Sigma-Aldrich. The water use throughout all experiments was purified through a Millipore system. All the chemicals were used as received without further purification.

Preparation of Ni_2S NSs: Ni_2S was prepared as follows. In a typical procedure, 5 mmol $\text{Ni}(\text{NO}_3)_2 \cdot 6\text{H}_2\text{O}$ and 10 mmol HMT were dissolved in 40 mL distilled water and stirred to form a clear solution. Then the aqueous solution was transferred to a 50 ml Teflon-lined stainless-steel autoclave. It was heated at 100 °C for 10 h to achieve the $\text{Ni}(\text{OH})_2$. After the autoclave cooled down naturally, the resulting precipitate was taken out and washed with distilled water and ethanol several times alternatively, followed by drying 6 h at 60 °C to obtain the hydroxide precursor. Next, S (1 g) was placed in the tube at the farthest upstream position and the $\text{Ni}(\text{OH})_2$ precursor was placed at center of the furnace. The sample was heated at 400 °C for 1 h with a heating speed of 2 °C min^{-1} under Ar atmosphere, and then cooled to room temperature naturally. Finally, the black Ni_2S NSs were collected for further characterization.

Characterizations: X-ray powder diffraction (XRD) patterns were measured using a Shimadzu XRD-6100 diffractometer (Shimadzu, Japan) with a Cu $K\alpha$ radiation.

Raman spectroscopy measurements were carried out on the LabRAM HR Evolution (Horiba) with an excitation wavelength of 532 nm. SEM images were obtained using a Quanta FEG 250 field-emission SEM with an accelerating voltage of 20 kV. TEM images were obtained from a Zeiss Libra 200FE transmission electron microscope operated at 200 kV. XPS measurements were performed on an ESCALABMK II X-ray photoelectron spectrometer using Mg as the exciting source. The absorbance data of spectrophotometer were acquired on SHIMADZU UV-1800 UV-Vis spectrophotometer.

Electrochemical measurements: An electrochemical workstation CHI 760E (CH Instruments, Inc., Shanghai) was employed to record the electrochemical response. The rotating ring disk electrode (RRDE) measurements were run at 25 °C in a typical three-electrode cell (RRDE (glassy carbon (GC) disk + Pt ring) as working electrode, Hg/HgO reference electrode (for alkaline solution) or Ag/AgCl reference (for acidic solution) as reference electrode, and a Pt mesh counter electrode). The potentials reported in this work were converted to reversible hydrogen electrode (RHE) scale via calibration with the following equation: $E \text{ (vs. RHE)} = E \text{ (vs. Ag/AgCl)} + 0.059 \times \text{pH} + 0.197 \text{ V}$ and the presented current density was normalized to the geometric surface area. For the accurate and reproducible measurement of H₂O₂ selectivity, it is very important to clean the RRDE thoroughly prior to each experiment. The RRDE was polished with 1 μm alumina aqueous suspension for 5 min and 0.05 μm alumina aqueous suspension for 5 min and ultra-sonicated in DI water for 20 s. Certain amounts of commercial H₂SO₄ was dissolved in Millipore water to prepare the 0.05 M

electrolyte. To prepare NiS₂ cast working electrode, typically, 5 mg of as-prepared NiS₂ catalyst was mixed with 0.8 mL of 2-propanol, 0.2 mL of H₂O and 30 μL of Nafion solution, and sonicated for 30 min to get a homogeneous catalyst ink. 8 μL of the ink was pipetted or spin-coated (100 rpm) onto glassy carbon disk (disk area of 0.246 cm², ring area of 0.186 cm²), got dried prior to usage. As the catalyst can be dispersed very well in ethanol solutions, uniform catalyst coating can be made on the disc electrode without obvious pinholes or uncovered edge. Before the linear sweep voltammetry (LSV) tests, cyclic voltammetry (CV) was performed between 0.2 and 1.20 V (vs. RHE) in N₂-saturated 0.1 M KOH at a scan rate of 100 mV s⁻¹ for around 50 cycles, in which a steady CV response was obtained. Pt ring was then electrochemically cleaned in the same potential range at a scan rate of 500 mV s⁻¹ for 10 cycles. O₂ gas was purged into the electrolyte for 10 min. The H₂O₂ production activity was assessed by RRDE scans from 0.0 to 0.7 V (vs. RHE) in O₂-saturated 0.05 M H₂SO₄ at a scan rate of 50 mV s⁻¹ and a rotation speed of 1600 rpm. During the LSV, the Pt ring potential was held at 1.2 V (vs. RHE). Polarization curves in N₂-saturated electrolyte were also recorded as a reference. H₂O₂ selectivity was calculated using the following equation: H₂O₂ (%) = 200 × (I_{Ring}/N) / (I_{Disk} + I_{Ring}/N), and the electron transfer number (n) at the disk electrode during ORR was calculated using $n = 4|I_{\text{Disk}}| / (I_{\text{Disk}} + I_{\text{Ring}}/N)$, where I_{Ring} is the ring current, I_{Disk} is the disk current and N is the collection efficiency (37.1% after calibration). The collection efficiency (N) was determined using the [Fe(CN)₆]^{3-/4-} redox system. The catalyst-deposited RRDE was soaked in N₂-saturated 0.1 M KNO₃ + 10 mM K₃[Fe(CN)₆], and

chronoamperometry was performed at -0.3 V (vs. Hg/HgO) while the ring potential was fixed at 0.5 V (vs. Hg/HgO) for 50 s. The background response was also obtained similarly, but the applied disk potential was 0.5 V (vs. Hg/HgO). The collection efficiency could be calculated as follows: $N = (i_r - i_{r,bg}) / i_d$, where $i_{r,bg}$ stands for the background ring current.

The electrogeneration of H_2O_2 : Bulk ORR electrolysis in 0.05 M H_2SO_4 and quantification of H_2O_2 concentration were carried out in a two-compartment cell under ambient condition, with 0.05 mg cm^{-2} NiS_2 catalyst dropped onto a 1×1 cm^2 carbon paper electrode as the ORR cathode. A Nafion 117 membrane was employed to separate the chambers. The membrane was protonated by first treating in H_2O_2 aqueous solution (5 wt%) at 80 °C for 1 h, then washed with deionized water until the pH value of the water returned to normal, followed by boiling with dilute H_2SO_4 (5 wt%) at 80 °C for 1 h. Finally, the membranes were soaked with deionized water for 4 h. The electrochemical experiments were carried out with an electrochemical workstation (CHI 760E) using a three-electrode configuration with prepared NiS_2/CP electrode, Pt mesh electrode and Ag/AgCl electrode as the working electrode, the counter electrode and the reference electrode, respectively. H_2O_2 yield was quantified by cerium sulfate titration based colorimetric method ($2Ce^{4+} + H_2O_2 \rightarrow 2Ce^{3+} + 2H^+ + O_2$) followed by Uv-Vis spectrophotometry. The absorption at 319 nm wavelength was measured on a SHIMADZU UV-1800 UV-Vis spectrophotometer and used to determine the Ce^{4+}/H_2O_2 concentration. The H_2O_2 concentration-absorbance curve was calibrated by a mixing known amount of

commercial H₂O₂ solution with 0.5 mM Ce(SO₄)₂. The fitting curve ($y = -0.0036x + 2.224618$, $R^2 = 0.989$) shows good linear relation of absorbance value with H₂O₂ concentration.

Details of density functional theory (DFT) calculations: The spin-polarization density functional theory (DFT) calculations were done via Vienna ab initio simulation package (VASP). The interaction between core electrons and ions was described with the projected augmented wave (PAW) pseudopotential^{1,2} and the exchange-correlation effect was accounted for with the Perdew, Burke, and Ernzerhof (PBE) functional.³ The DFT+D3 method has been adopted to describe the van der Waals interactions.⁴ The plane-wave basis with the kinetic energy cutoff of 450 eV was used. The convergence criteria for the total energy and the Hellmann-Feynman force were 10⁻⁵ eV and 0.02 eVÅ⁻¹, respectively. The NiS₂ (200) (2×2) supercell, as shown in Fig. S1, was adopted with a vacuum layer of ~ 15 Å for modelling the two-electron ORR. For the NiS₂ bulk and the NiS₂ (200) (2×2) supercell, 8×8×8 and 3×3×1 Monkhorst-Pack grids⁵ were adopted, respectively. With these computational settings, the optimized lattice parameter (5.576 Å) agrees well with the previous theoretical value (5.57 Å)⁶. The computational hydrogen electrode model has been adopted for calculations of the Gibbs free-energy change for the relevant elemental steps,⁷ which can be obtained by the following equation: $\Delta G = \Delta E + \Delta E_{ZPE} - T\Delta S$. The total energy (E), zero-point energy (E_{ZPE}), and entropy (S) of the adsorbed intermediates were obtained from DFT calculations, while the thermodynamic corrections of the free molecules taken from the NIST databases.⁸ The theoretical

overpotential (η) of two-electron ORR was deduced using the equation of $\eta = |\Delta G_{\text{HOO}^*}/e - 4.22 \text{ V}|$. The solvation effect was not considered in determining the value of ΔG_{HOO^*} , which governs a reasonable comparison, as previous works.⁹⁻¹¹ Note that the consideration of solvation effect, which may bring a small stabilization (0.1~0.2 eV) on HOO^* , should not change the reported activity trend in this work and previous studies.⁹⁻¹¹

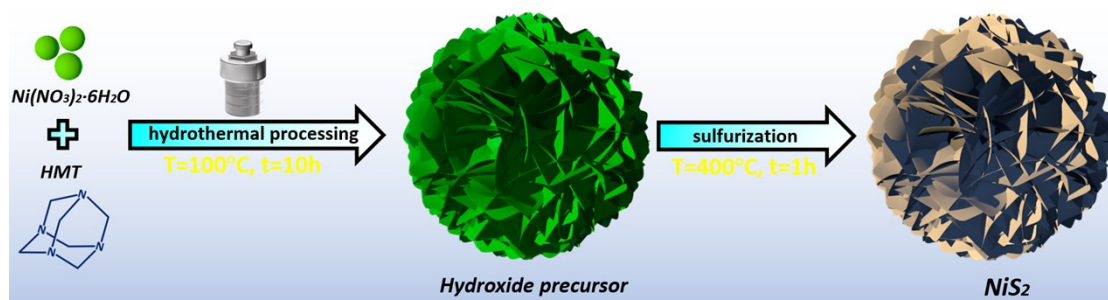


Fig. S1. Schematic illustration for the preparation of NiS₂.

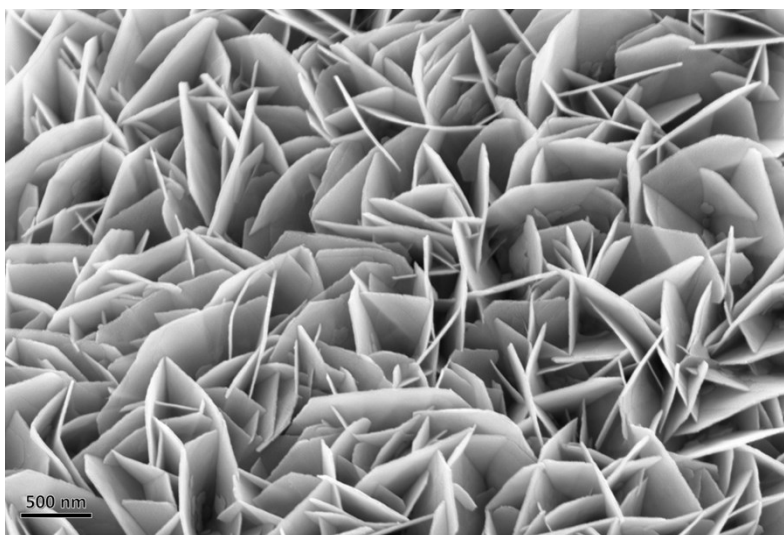


Fig. S2. SEM image for the hydroxide precursor of NiS_2 .

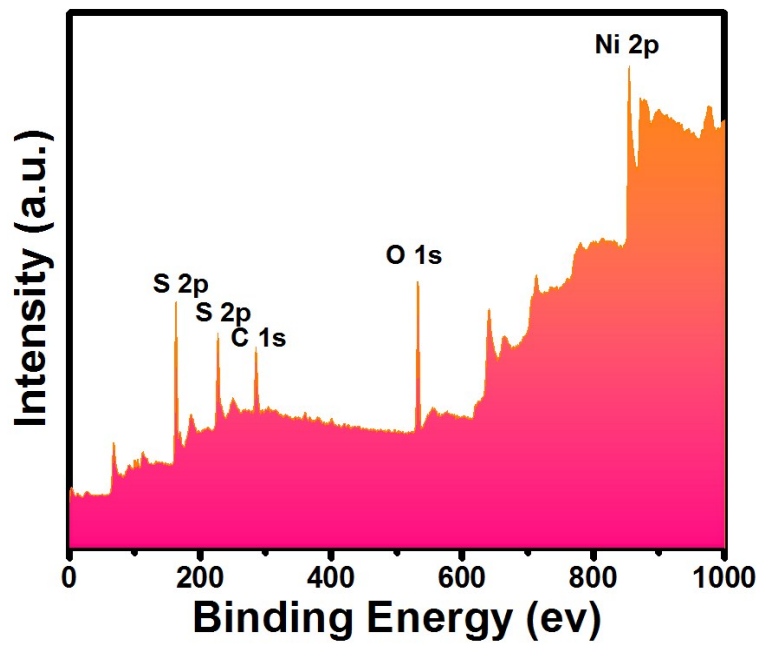


Fig. S3. XPS survey spectrum for NiS₂.

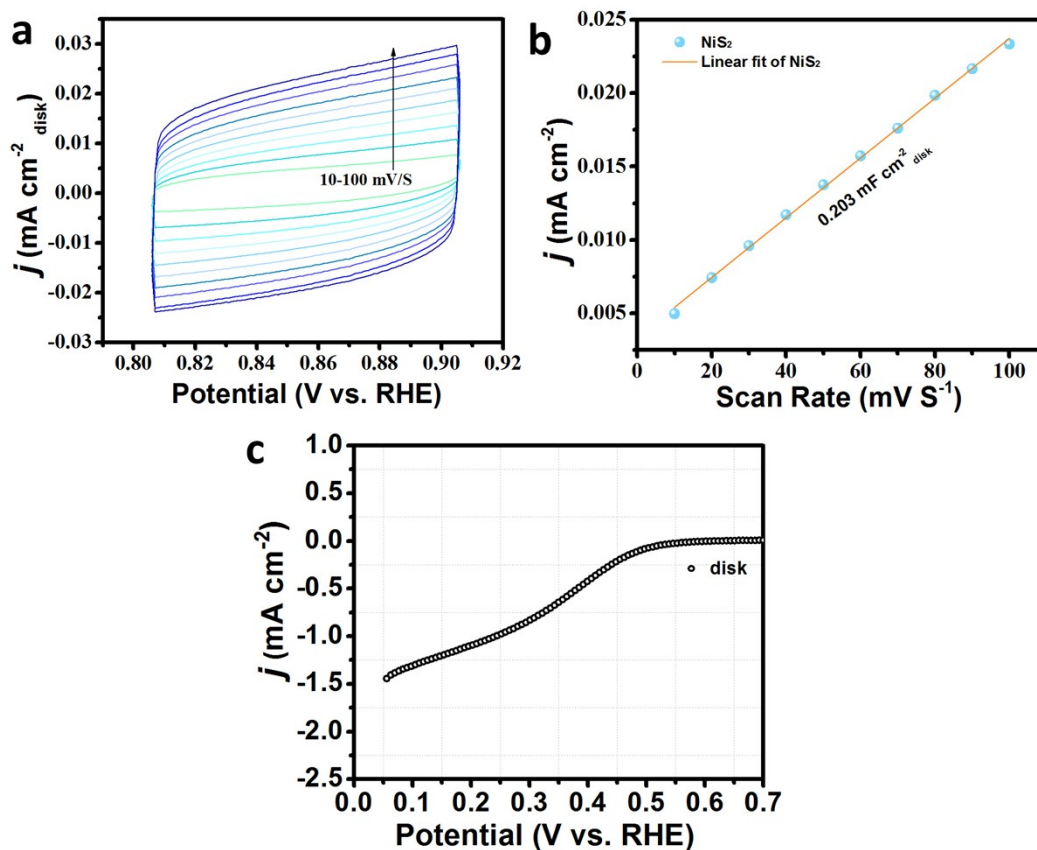


Fig. S4. (a) Cyclic voltammogram (CV) curves for NiS₂ in the double layer region at scan rates of 10, 20, 30, 40, 50, 60, 70, 80, 90, and 100 mV s⁻¹ in 0.05 M H₂SO₄ aqueous electrolyte. (b) Current (taken at the potential of 0.856 V vs. RHE) as a function of scan rate derived from (a). The double-layer capacitance (C_{dl}) for NiS₂ is 0.203 mF cm⁻²_{disk}. (c) Polarization curve (disk current) for NiS₂ in 0.05 M H₂SO₄ after ECSA normalization.

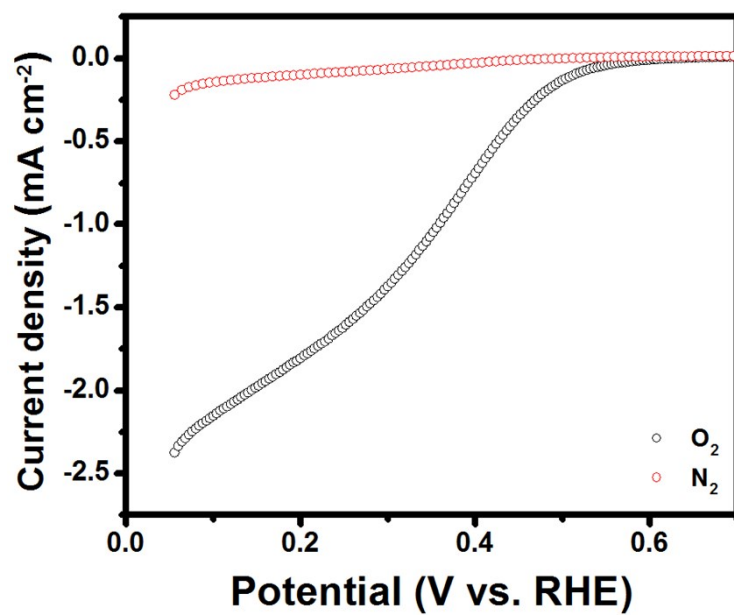


Fig. S5. Polarization curves for NiS₂ at 1600 rpm in O₂- and N₂-saturated 0.05 M H₂SO₄.

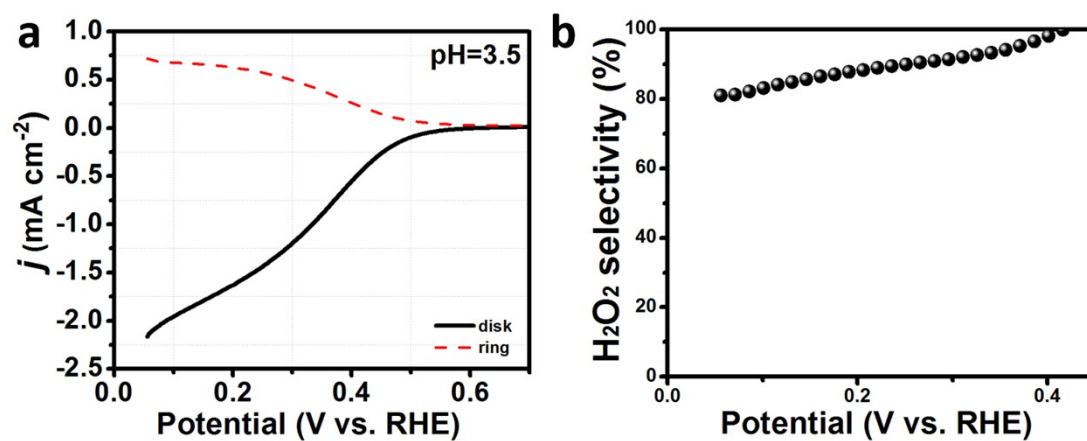


Fig. S6. (a) Polarization curves for NiS₂ at a higher pH value of 3.5. (b) Calculated H₂O₂ selectivity.

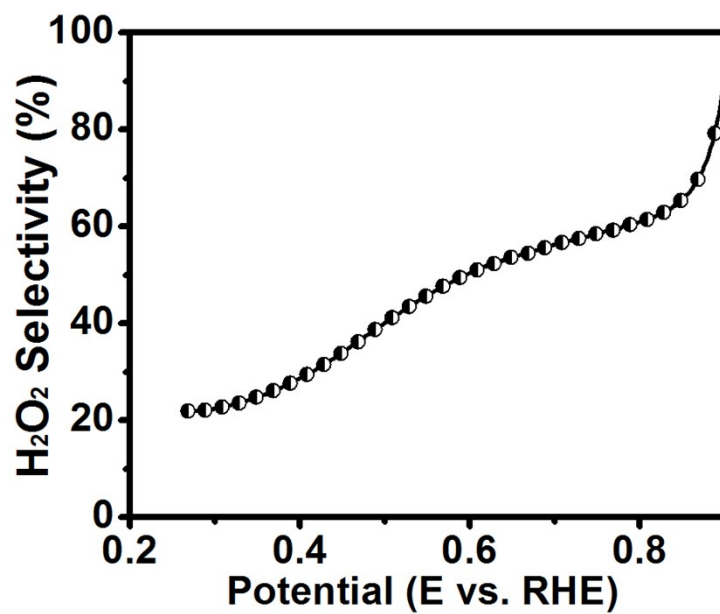


Fig. S7. H₂O₂ selectivity for NiS₂ measured in O₂-saturated 0.1 M KOH at an electrode rotation speed of 1600 rpm.

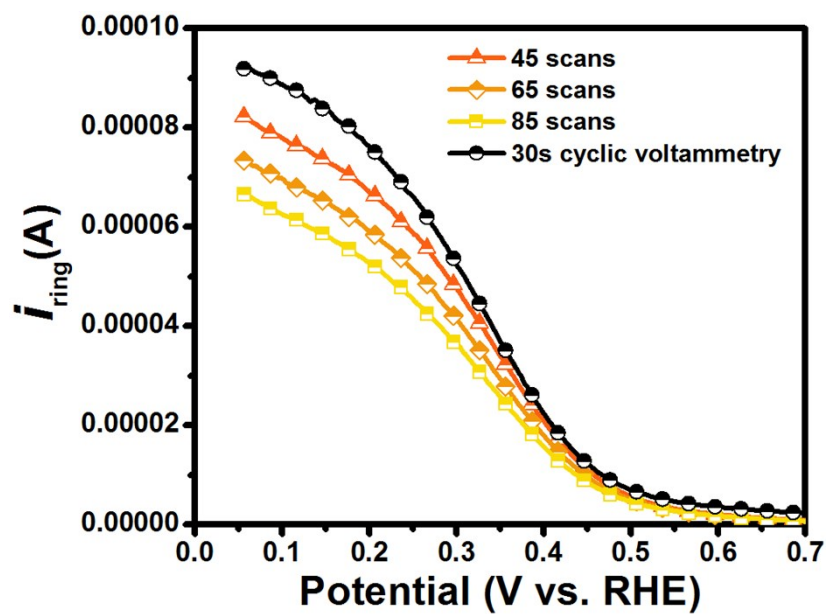


Fig. S8. Typical trend in ring current for NiS₂ at 1600 rpm in 0.05 M H₂SO₄ over consecutive scans (recovered after cyclic voltammetry cleaning).

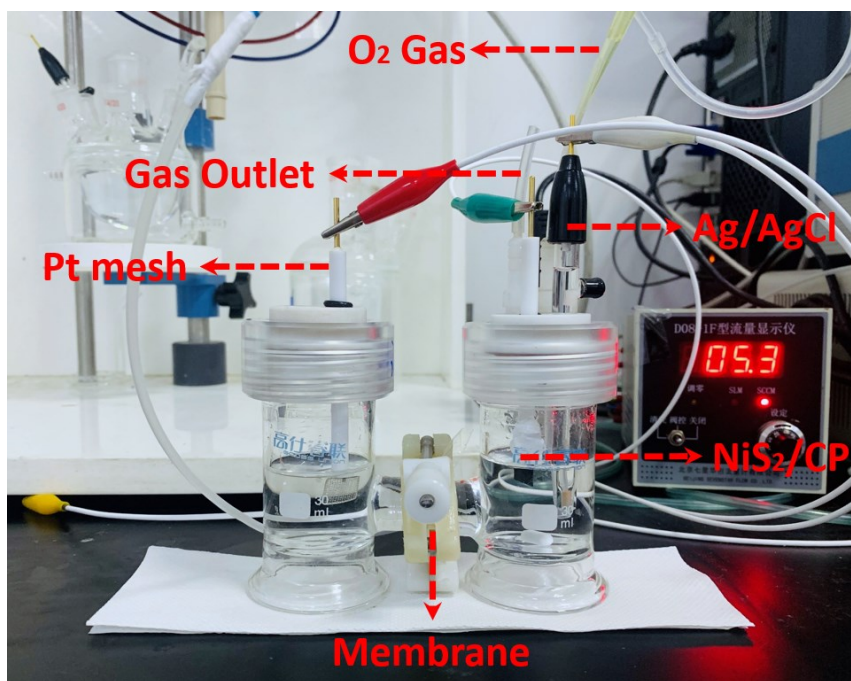


Fig. S9. Optical photograph for the H-cell reactor.

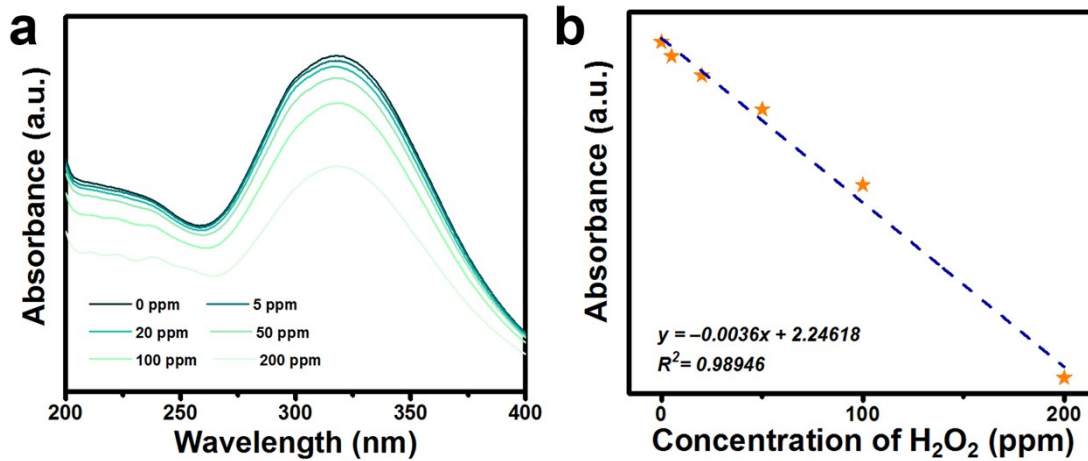


Fig. S10. (a) UV-Vis absorption spectra of various H₂O₂ concentrations after incubated for one hour at room temperature. (b) Calibration curve used for calculation of H₂O₂ concentrations.

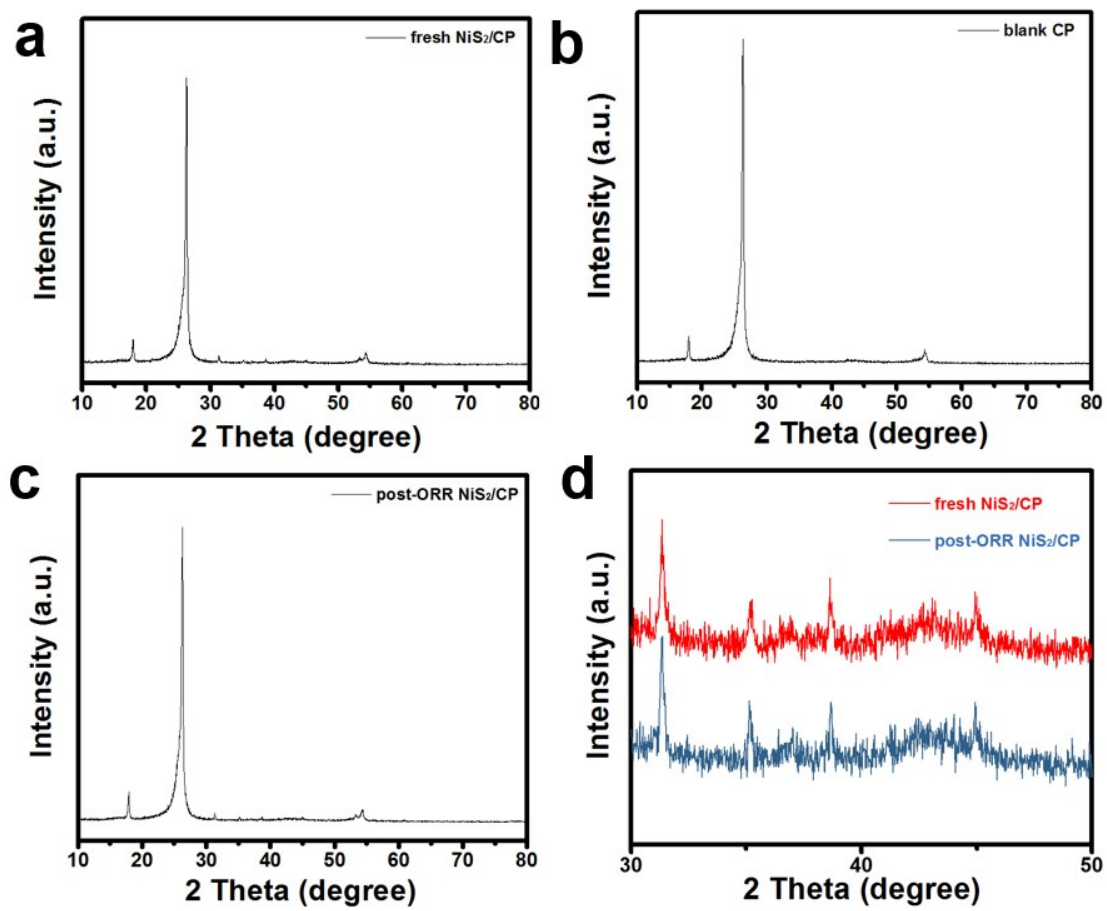


Fig. S11. XRD patterns for (a) fresh NiS₂/CP and (b) blank CP and (c) post-ORR NiS₂/CP. (d) XRD comparison of fresh NiS₂/CP and post-ORR NiS₂/CP.

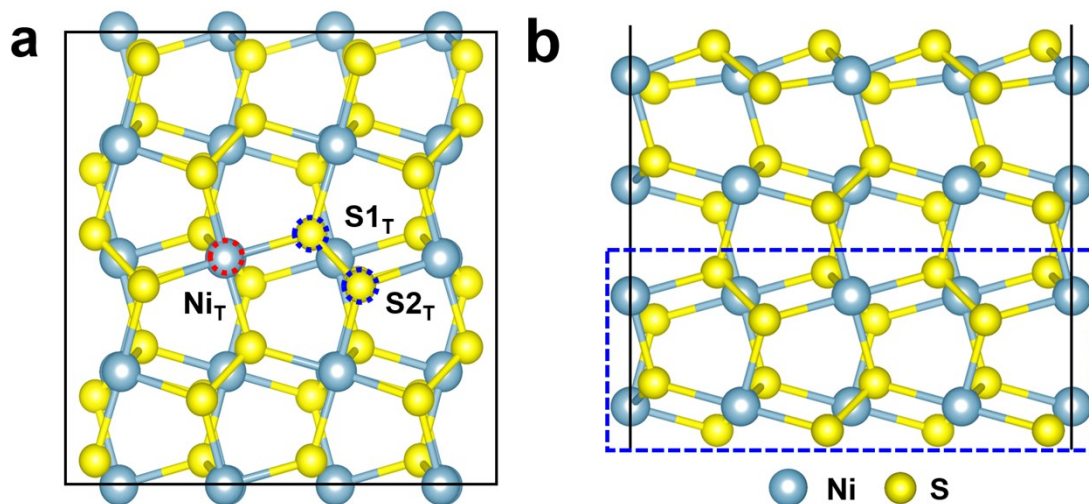


Fig. S12. Top (a) and side (b) views of the NiS_2 (100) (2×2) surface, where the solid lines denote the boundary of the supercell. The slab model contains four repeated units, in which the bottom two ones (enclosed with the dashed lines) are fixed to mimic the bulk. In (a), the considered adsorption sites (Ni_T , S1_T and S2_T) for the OOH species are marked by the dotted circles. The blue and yellow spheres denote the Ni and S atoms, respectively.

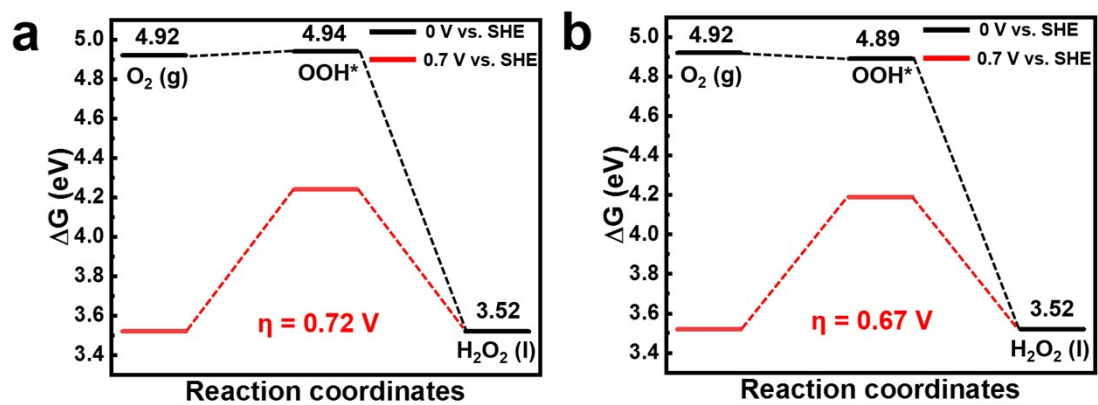


Fig. S13. Free energy diagrams with the theoretical overpotentials (η) of the 2e⁻ ORR at the zero potential (black line) and the equilibrium potential (red line) of $U_{O_2/H_2O_2} = 0.70$ V for the S1_T (a) and S2_T (b) sites, which are marked in Fig. S12.

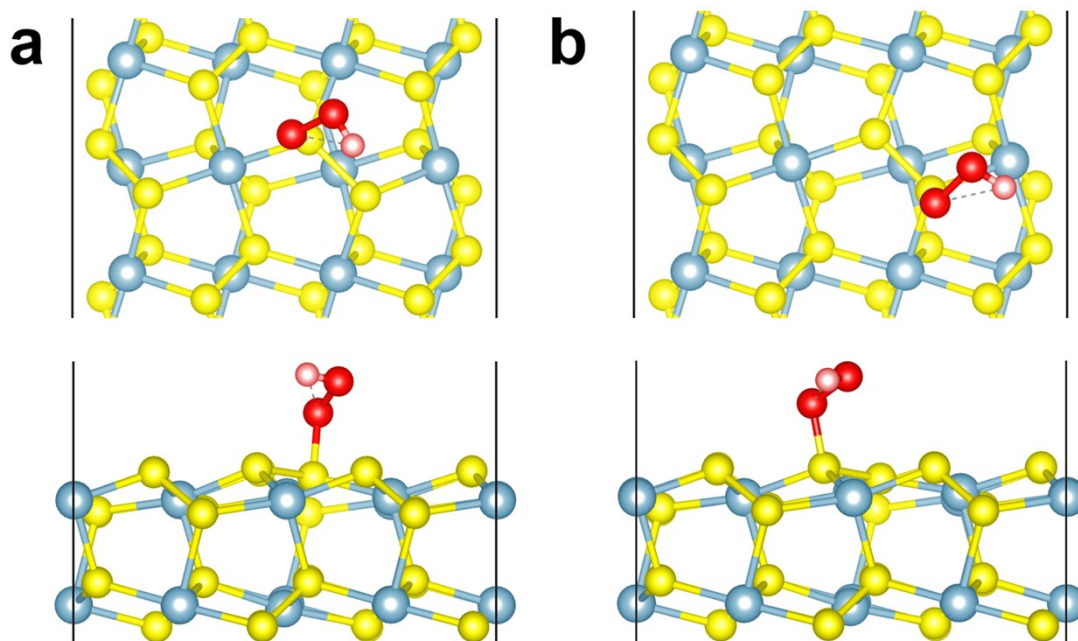


Fig. S14. Top and side views of the obtained configurations for the OOH species adsorption at $S1_T$ (a) and $S2_T$ (b) sites. The blue, yellow, red, and pink spheres denote the Ni, S, O, and H atoms, respectively.

Table S1. Comparison of NiS_2 with reported $2e^-$ ORR catalysts for H_2O_2 production in acidic solutions (“As” for Au/C-35 and $Au_{0.92}Pd_{0.08}/C$ refers to surface area of metals with respect to one gram of the metals/C catalyst).

Catalyst	Selectivity (%@V vs. RHE)	pH	Accumulation (mg L ⁻¹ @V vs. RHE)	Stability	Mass loading (mg cm ⁻²)	Surface area (m ² g ⁻¹) or C _{dl} (mF cm ⁻² disk)	Ref.
NiS ₂	99%@0.4	1	109@0.156 V (60 min)	6 h (H-cell)	0.05	C _{dl} =0.203	This work
Pt-Hg/C	90@0.4	1	N/A	8000 cycles	0.014	N/A	9
Au/C-35	80%@0.1	1	N/A	N/A	N/A	A _S =7.7 m ² g ⁻¹	12
Pt/HSC	94@0.5	1	2.64@0V (60 min)	6 h	0.05	~2800	13
C(Pt)/C	41@0.1	0	N/A	7000 cycles	0.08	N/A	14
CoSe ₂	~70%@0.45	1.2	91.16@0.5V (60min)	~4h	0.305	C _{dl} =0.325 (in 0.05 M H ₂ SO ₄)	15
FPC-800	80@0.1	1	112.6–792.6 mmol g ⁻¹ (60min)	24h	0.86	1001.8–1274.7	16
Pd ₂ Hg ₅ /C	~90@0.3	1	N/A	8000 cycles	N/A	N/A	17
meos-BMP-800	65.2@0.1	1	~0.26 mg (60min)	5.74 h	0.325	~320	18
RF-AQ-XC72	83%@0	1	18@0.1 V (60 min)	N/A	2.5	N/A	19
FePc/C	~80@-0.26	0.7	230@-1V (60min)	N/A	N/A	N/A	20
O-CNTs	52.5%@0.1	1	N/A	N/A	0.1	N/A	21
Pt/TiN	55%@0.33	1	N/A	1h	0.175	N/A	22
Mn-O/N@NCs	74@0.2	1	N/A	N/A	N/A	32.33–71.58	23
Co-N-C	~75%@0.3	0.3	N/A	N/A	0.1	315–430	24
Co ₁ -NG(O)	43%@0.55	1	N/A	N/A	0.01	C _{dl} =74.68 F g ⁻¹	25
CoS ₂	70%@0.5	1.26	148@0.5 V (60 min)	N/A	0.305	C _{dl} =0.169 (in 0.05 M H ₂ SO ₄)	26
MoTe ₂ /Graphene	~90%@0.3	~0	N/A	5000 cycles	for MoTe ₂ , 0.01	N/A	27
{001}-Fe ₂ O _{3-x}	91%@0.3	2.7	N/A	N/A	3.0	41.9, C _{dl} =0.48	28
N-doped mesoporous carbon	95%@0.3	0.3	N/A	N/A	0.2	782–1152	29
NCMK3IL 50_800T	95.2%@0.1	0.3	159.9 mmol g _{catalyst} ⁻¹ (60min)	6 h	0.05	1541	30
monodisperse colloidal PtP ₂ NCs	~90%@0.35	1	2.26 mmol cm ⁻² (60min) (pH = 6.6)	N/A	N/A	238	31

PEI50CMK 3_800T	98.5%@0.35	0.3	N/A	N/A	0.05	726–1682	32
h-Pt ₁ -CuS _x	92%@0.05	1	546±30 mol kg _{cat} ⁻¹ (60 min)	10000 cycles	0.015	N/A	33
Au _{0.92} Pd _{0.08} / C	95%@0	1	N/A	N/A	0.11	A _S =5.7 m ² g ⁻¹	34
g-N-CNHs	~90%@0.2	1	N/A	6 h	0.07	481	35
meso-BMP	20%@0.1	1	~5@0.1 V (60 min)	N/A	0.307	320	36
Co/carbon	~80%@0.4	0	5 μmmol cm ⁻² (60min)	N/A	0.6	N/A	37
CoN@CNT s	97.5@0.50	1	633.25@0.3 V (60 min)	12h	0.25	N/A	38
Pd ^{δ+} -OCNT	92%@0.35	1	1701 mol Kg _{cat} ⁻¹ (60min)	8.3h	0.1	163.3	39
Pt/TiC	~70@0.2	1	N/A	1000 cycles	0.0225	N/A	40

References

- 1 P. E. Blöchl, *Phys. Rev. B*, 1994, **50**, 17953-17979.
- 2 G. Kresse and J. Furthmüller, *Phys. Rev. B*, 1996, **54**, 11169.
- 3 J. P. Perdew, K. Burke and M. Ernzerhof, *Phys. Rev. Lett.*, 1996, **77**, 3865-3868.

- 4 S. Grimme, J. Antony, S. Ehrlich and H. Krieg, *J. Chem. Phys.*, 2010, **132**, 154104.
- 5 H. J. Monkhorst and J. D. Pack, *Phys. Rev. B*, 1976, **13**, 5188-5192.
- 6 M.-H. Wu, W.-J. Chou, J.-S. Huang, D. B. Putungan and S.-H. Lin, *Phys. Chem. Chem. Phys.*, 2019, **21**, 21561-21567.
- 7 J. K. Nørskov, J. Rossmeisl, A. Logadottir, L. Lindqvist, J. R. Kitchin, T. Bligaard and H. Jónsson, *J. Phys. Chem. B*, 2004, **108**, 17886-17892.
- 8 <http://webbook.nist.gov/chemistry/>.
- 9 S. Siahrostami, A. Verdaguier-Casadevall, M. Karamad, D. Deiana, P. Malacrida, B. Wickman, M. Escudero-Escribano, E. A. Paoli, R. Frydendal, T. W. Hansen, I. Chorkendorff, I. E. L. Stephens and J. Rossmeisl, *Nat. Mater.*, 2013, **12**, 1137-1143.
- 10 Z. Lu, G. Chen, S. Siahrostami, Z. Chen, K. Liu, J. Xie, L. Liao, T. Wu, D. Lin, Y. Liu, T. F. Jaramillo, J. K. Nørskov and Y. Cui, *Nat. Catal.*, 2018, **1**, 156-162.
- 11 X. Zhao, Y. Wang, Y. Da, X. Wang, T. Wang, M. Xu, X. He, W. Zhou, Y. Li, J. N. Coleman and Y. Li, *Natl. Sci. Rev.*, 2020, **7**, 1360-1366.
- 12 J. S. Jirkovský, M. Halasa and D. J. Schiffrin, *Phys. Chem. Chem. Phys.*, 2010, **12**, 8042-8053.
- 13 C. H. Choi, M. Kim, H. C. Kwon, S. J. Cho, S. Yun, H.-T. Kim, K. J. J. Mayrhofer, H. Kim and M. Choi, *Nat. Commun.*, 2016, **7**, 10922.
- 14 C. H. Choi, H. C. Kwon, S. Yook, H. Shin, H. Kim and M. Choi, *J. Phys. Chem. C*, 2014, **118**, 30063-30070.
- 15 H. Sheng, A. N. Janes, R. D. Ross, D. Kaiman, J. Huang, B. Song, J. R. Schmidt and S. Jin, *Energy Environ. Sci.*, 2020, **13**, 4189-4203.
- 16 K. Zhao, Y. Su, X. Quan, Y. Liu, S. Chen and H. Yu, *J. Catal.*, 2018, **357**, 118-126.
- 17 A. Verdaguier-Casadevall, D. Deiana, M. Karamad, S. Siahrostami, P. Malacrida, T. W. Hansen, J. Rossmeisl, I. Chorkendorff and I. E. L. Stephens, *Nano Lett.*, 2014, **14**, 1603-1608.
- 18 T.-P. Fellerger, F. Hasché, P. Strasser and M. Antonietti, *J. Am. Chem. Soc.*,

- 2012, **134**, 4072-4075.
- 19 A. Wang, A. Bonakdarpour, D. P. Wilkinson and E. Gyenge, *Electrochim. Acta*, 2012, **66**, 222-229.
- 20 F. L. Silva, R. M. Reis, W. R. P. Barros, R. S. Rocha and M. R. V. Lanza, *J. Electroanal. Chem.*, 2014, **722-723**, 32-37.
- 21 Z. Lu, G. Chen, S. Siahrostami, Z. Chen, K. Liu, J. Xie, L. Liao, T. Wu, D. Lin, Y. Liu, T. F. Jaramillo, J. K. Nørskov and Y. Cui, *Nat. Catal.*, 2018, **1**, 156-162.
- 22 S. Yang, J. Kim, Y. J. Tak, A. Soon and H. Lee, *Angew. Chem. Int. Ed.* 2016, **55**, 2058-2062.
- 23 A. Byeon, J. Cho, J. M. Kim, K. H. Chae, H.-Y. Park, S. W. Hong, H. C. Ham, S. W. Lee, K. R. Yoon and J. Y. Kim, *Nanoscale Horiz.*, 2020, **5**, 832-838.
- 24 Y. Sun, L. Silvioli, N. R. Sahraie, W. Ju, J. Li, A. Zitolo, S. Li, A. Bagger, L. Arnarson, X. Wang, T. Moeller, D. Bernsmeier, J. Rossmeisl, F. Jaouen and P. Strasser, *J. Am. Chem. Soc.*, 2019, **141**, 12372-12381.
- 25 E. Jung, H. Shin, B.-H. Lee, V. Efremov, S. Lee, H. S. Lee, J. Kim, W. Hooch Antink, S. Park, K.-S. Lee, S.-P. Cho, J. S. Yoo, Y.-E. Sung and T. Hyeon, *Nat. Mater.*, 2020, **19**, 436-442.
- 26 H. Sheng, E. D. Hermes, X. Yang, D. Ying, A. N. Janes, W. Li, J. R. Schmidt and S. Jin, *ACS Catal.*, 2019, **9**, 8433-8442.
- 27 X. Zhao, Y. Wang, Y. Da, X. Wang, T. Wang, M. Xu, X. He, W. Zhou, Y. Li, J. N. Coleman and Y. Li, *Nat. Sci. Rev.*, 2020, **7**, 1360-1366.
- 28 R. Gao, L. Pan, Z. Li, C. Shi, Y. Yao, X. Zhang and J.-J. Zou, *Adv. Funct. Mater.*, 2020, **30**, 1910539.
- 29 J. Park, Y. Nabae, T. Hayakawa and M.-a. Kakimoto, *ACS Catal.*, 2014, **4**, 3749-3754.
- 30 Y. Sun, I. Sinev, W. Ju, A. Bergmann, S. Dresp, S. Kühn, C. Spöri, H. Schmies, H. Wang, D. Bernsmeier, B. Paul, R. Schmack, R. Kraehnert, B. Roldan Cuenya and P. Strasser, *ACS Catal.*, 2018, **8**, 2844-2856.
- 31 H. Li, P. Wen, D. S. Itanze, Z. D. Hood, S. Adhikari, C. Lu, X. Ma, C. Dun, L. Jiang, D. L. Carroll, Y. Qiu and S. M. Geyer, *Nat. Commun.*, 2020, **11**, 3928.

- 32 Y. Sun, S. Li, Z. P. Jovanov, D. Bernsmeier, H. Wang, B. Paul, X. Wang, S. Kühl and P. Strasser, *ChemSusChem*, 2018, **11**, 3388-3395.
- 33 R. Shen, W. Chen, Q. Peng, S. Lu, L. Zheng, X. Cao, Y. Wang, W. Zhu, J. Zhang, Z. Zhuang, C. Chen, D. Wang and Y. Li, *Chem*, 2019, **5**, 2099-2110.
- 34 J. S. Jirkovský, I. Panas, E. Ahlberg, M. Halasa, S. Romani and D. J. Schiffrin, *J. Am. Chem. Soc.*, 2011, **133**, 19432-19441.
- 35 D. Iglesias, A. Giuliani, M. Melchionna, S. Marchesan, A. Criado, L. Nasi, M. Bevilacqua, C. Tavagnacco, F. Vizza, M. Prato and P. Fornasiero, *Chem*, 2018, **4**, 106-123.
- 36 F. Hasché, M. Oezaslan, P. Strasser and T.-P. Feller, *J. Energy Chem.*, 2016, **25**, 251-257.
- 37 A. Bonakdarpour, D. Esau, H. Cheng, A. Wang, E. Gyenge and D. P. Wilkinson, *Electrochim. Acta*, 2011, **56**, 9074-9081.
- 38 Q. Zhang, X. Tan, N. M. Bedford, Z. Han, L. Thomsen, S. Smith, R. Amal and X. Lu, *Nat. Commun.*, 2020, **11**, 4181.
- 39 Q. Chang, P. Zhang, A. H. B. Mostaghimi, X. Zhao, S. R. Denny, J. H. Lee, H. Gao, Y. Zhang, H. L. Xin, S. Siahrostami, J. G. Chen and Z. Chen, *Nat. Commun.*, 2020, **11**, 2178.
- 40 S. Yang, Y. J. Tak, J. Kim, A. Soon and H. Lee, *ACS Catal.*, 2017, **7**, 1301-1307.